Available online at www.sciencedirect.com
SCIENCE DIRECT®
ELSEVIER
European Journal of Mechanics B/Fluids 23 (2004) 209–218
EUROPEAN JOURNAL OF MECHANICS B/FLUIDS

Multi-modal Vortex-Induced Vibrations of a vertical riser pipe subject to a uniform current profile

Richard H.J. Willden [a,*], J. Michael R. Graham [b]

[a] *Department of Engineering, University of Cambridge, CB2 1PZ, UK*
[b] *Department of Aeronautics, Imperial College London, SW7 2AZ, UK*

Received 4 April 2003; received in revised form 19 September 2003; accepted 22 September 2003

Abstract

The transverse Vortex-Induced Vibrations of a long (length to diameter ratio, $L/D = 1544$), flexible pipe, that was subjected to a uniform current profile (Reynolds number, $Re = 2.84 \times 10^5$) have been simulated using a strip theory Computational Fluid Dynamics model. The pipe's mass ratio (the ratio of the pipe's mass to the mass of fluid displaced by it) was varied between 1.0 and 3.0 in order to study its effect upon the vibrational behaviour of the pipe. Despite the inflow current being uniform the pipe was observed to vibrate multi-modally. Furthermore, all of the excited modes vibrated at the excitation (Strouhal) frequency. The fluid, via its added mass, was found to be able to excite modes whose natural frequencies differed from the excitation frequency. This ability was observed to decrease with increasing mass ratio.

Keywords: Riser pipes; Vortex-Induced Vibration; Computational Fluid Dynamics; Multi-modal vibration; Added mass

1. Introduction

For all but the lowest Reynolds numbers the flow past a circular cylinder results in the asymmetric shedding of vortices into the cylinder's wake. The vortices induce periodic forces on the cylinder. These forces can cause an elastically supported cylinder to vibrate. Such a vibration is termed a Vortex-Induced Vibration (VIV).

The amplitude of vibration is dependent upon the level of structural damping, the mass ratio (the ratio of the body's mass to the mass of fluid displaced by it) and the proximity of the frequency of the fluid forces to the body's natural frequency of vibration. The fluid forces in both the cross-stream (transverse) direction, the lift, and the streamwise (in-line) direction, the drag, can induce VIV in their respective directions. Transverse VIV is usually of larger amplitude than in-line VIV, as the oscillatory component of the lift force is normally greater than that of the drag force. Transverse VIV can exceed one diameter in amplitude.

Long elastic cylinders, such as marine riser pipes, may exhibit VIV when exposed to current flows. The fluid excitation of a flexible pipe results in modal vibrations. Riser pipes are often exposed to high Reynolds number currents, $Re > 10^5$ (where $Re = UD/\nu$ is the Reynolds number and U, D and ν are the free stream flow speed, the diameter of the pipe and the kinematic viscosity of the fluid respectively), and are being deployed in increasingly deeper waters (>2000 m depth), resulting in high mode number vibrations (>20th mode). Such vibrations can be of serious consequence as they provide a potent source of fatigue and can, together with wake interactions, cause pipe clashing in multiple pipe assemblies.

Due in part to its potentially destructive consequences VIV has received considerable research attention. The reader is referred to the review papers by Sarpkaya [1], Bearman [2] and Parkinson [3], and also to the recent papers by Khalak and

* Corresponding author. Present address: Department of Aeronautics, Imperial College London, SW7 2AZ, UK.
E-mail address: r.willden@imperial.ac.uk (R.H.J. Willden).

0997-7546/$ – see front matter
doi:10.1016/j.euromechflu.2003.09.011

Williamson [4] and Govardhan and Williamson [5], which are concerned with the VIV of low mass ratio cylinders, for a comprehensive review of recent works relating to VIV.

Conventional wisdom suggests that a pipe can only be excited into multi-modal VIV if the excitation frequency (the vortex shedding frequency) varies along the pipe's length. For a straight, constant diameter pipe this implies that a sheared onset current profile is required to enable multiple modes to become simultaneously excited. This claim is the subject of investigation of this paper.

The paper presents the results of a series of (strip theory) Computational Fluid Dynamics (CFD) simulations of the transverse VIV of a riser pipe that was subjected to a uniform current profile. The riser pipe was of realistic geometry, length to diameter ratio $L/D = 1544$, and the current of realistic Reynolds number, $Re = 2.84 \times 10^5$. The mass ratio, m^*, was varied within realistic bounds, $1.0 \leqslant m^* \leqslant 3.0$, in order to study its effect upon the VIV behaviour of the pipe.

2. Numerical method

A coupled fluid and structural dynamics model, VIVIC, is used to simulate the response of the riser in the time domain. The numerical method is briefly summarised here; see Willden and Graham [6] or Willden [7] for further details.

2.1. Computational Fluid Dynamics

A CFD model, which is based upon strip theory, is used to simulate the fluid dynamics. Strip theory entails computing the fluid flow in multiple two-dimensional planes that are positioned at intervals along the length of a body. A suitable choice for the number of simulation planes can be made by considering the highest mode of vibration that is likely to be excited. The highest expected mode of vibration can be approximately determined as the mode whose natural frequency of vibration least exceeds the maximum Strouhal frequency in the onset current profile. Given the highest expected mode number one needs to consider how the flow might vary across each half wave-length of pipe vibration. The three-dimensional flexible pipe simulations of Newman and Karniadakis [8] showed that towards the nodes of a transversely vibrating pipe the fluid acts to excite the pipe's vibration, whereas towards the anti-nodes the fluid provides hydrodynamic damping. Hence, a minimum of three simulation planes are required per half wave-length of pipe vibration in order to correctly capture the axial variation of the phasing of the fluid forces with respect to the pipe's motion. 64 simulation planes, positioned equidistantly along the pipe's axis, are used in the present computations, as this provides a minimum of three simulation planes per half-wavelength for modes up to and including those of natural frequency equal to twice the Strouhal frequency of the onset current profile. The topology of the CFD model is depicted in Fig. 1.

The model assumes that the flow is locally two-dimensional. Although the flow past a stationary circular cylinder develops three-dimensional vortical structures for $Re > 180$ (see Williamson [9]), an effect of lock-in (the synchronisation of the vortex shedding and oscillatory frequencies) is to correlate the vortex shedding along substantial lengths of the pipe (see Toebes [10]), rendering the local fluid flow predominantly two-dimensional.

The velocity-vorticity formulation of the two-dimensional incompressible Navier–Stokes equations is solved in each simulation plane using a hybrid Eulerian–Lagrangian Vortex-in-Cell method. A time split approach is followed whereby the diffusion of vorticity is treated in an Eulerian fashion by modelling the flow variables using linear Finite Elements on an unstructured mesh. The convection of vorticity is handled using a Lagrangian approach that employs discrete point vortices. The two-dimensional solver originated as a Vortex-in-Cell method (Graham [11]) that employed finite difference approximations and fast Fourier transforms on a structured grid.

A Large Eddy Simulation (LES) model is used to model the effects of turbulent length scales at high Reynolds numbers. The LES model uses a simple volume average box filter to separate the resolvable and sub-grid flow scales. The resulting sub-grid scale stresses are approximated using a gradient diffusion model proposed by Smagorinsky [12]. Fig. 2 presents Strouhal numbers, St, and root mean square lift coefficients, $C_{L\text{rms}}$, computed using the LES model for a rigid cylinder over a subcritical Reynolds number range. For comparative purposes experimental data from Norberg [13] is also presented in this figure. The agreement in both St and $C_{L\text{rms}}$ is good over the Reynolds number range 2×10^4 to 2×10^5, which encompasses the range of practical interest.

The motion of the body is accounted for in each simulation plane by making use of the kinematic equivalence of the accelerating (body fixed) and inertial (absolute) frames of reference. This equivalence allows the motion of the body through the fluid to be simulated in the local body fixed frame of reference with a time dependent incident velocity that is equal to the local relative velocity of the current to the body in the inertial frame.

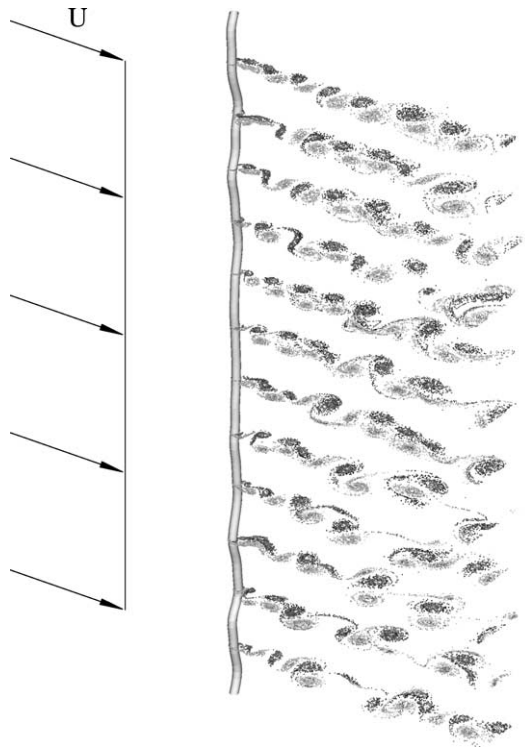

Fig. 1. A vortex particle image of the wake behind a transversely vibrating vertical riser (not to scale). For clarity not all of the CFD simulation planes are shown in the figure. The shade of the particles indicates the sign of the vorticity; lighter shades represent positive vorticity whilst darker shades represent negative vorticity.

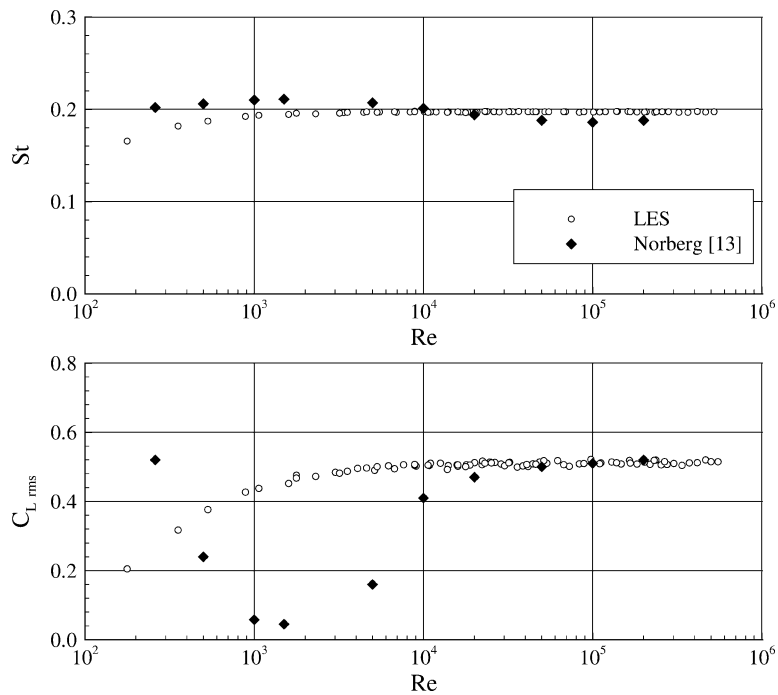

Fig. 2. Simulated, using Large Eddy Simulation (LES) and experimental, from Norberg [13], Strouhal number, *St*, and root mean square lift coefficient, $C_{L\mathrm{rms}}$, variation with Reynolds number, *Re*, for a stationary circular cylinder.

2.2. Structural dynamics

A linear Finite Element implementation of the Bernoulli–Euler bending beam equations is used to model the response of the structure to the fluid loading. The structure is discretised into elements across which cubic interpolation functions are used to represent the pipe's transverse response. The pipe's axial stress varies spatially due to the effects of the pipe's weight and buoyancy force. However, the axial stress distribution is not permitted to vary in time due to bending motions. The structural model is therefore referred to as linear. Structural damping is modelled using a proportional damping model.

In the forthcoming discussion of the simulation results references are made to the structure's natural modes of vibration. These modes and their associated natural frequencies are determined by solving the structure's eigen-problem in isolation. Hence, no fluid added mass is included with the structural mass and the natural frequencies and mode shapes are those of the riser in a vacuum.

In the present simulations the structural damping was set to 0.3% of critical for all modes of vibration. Additionally, the riser's top and bottom attachments were modelled as pin jointed and a top tension equal to twice the weight of water displaced by the pipe was applied.

2.3. Fluid–structure interaction

Each time step commences by mapping the transverse hydrodynamic force at the start of the step to the nodes of the structural model. This is accomplished by using cubic spline interpolations with reflective boundary conditions at the free surface and the seabed. The structural model uses this loading to explicitly compute the pipe's motion. Each simulation plane accounts for the pipe's motion in an accelerating reference frame by appropriately perturbing the plane's incident flow at the end of the step. The CFD model is advanced in time using a semi-implicit integration scheme, yielding the fluid loading at the end of the step. The simulation proceeds by repeating the above steps. Note that three-dimensional coupling is solely provided through the pipe's motion.

The combined fluid-structure interaction model has been validated, see Willden and Graham [14] or Willden [7], against experimental data from model Steel Catenary Riser (SCR) towing tests, conducted at MARINTEK [15]. The simulated VIV displacements in both the in-plane and out-of-plane directions were found to be in very good agreement with those determined experimentally. Note that in addition to the computational method described above the VIV simulation of an SCR requires the prior determination of the deformation of the pipe due to its weight, buoyancy force and the mean drag force acting on it. Such a deformed configuration can only be computed using a non-linear structural dynamics model.

3. Simulation results

Six mass ratios have been simulated: $m^* = 1.0$, 1.25, 1.5, 2.0, 2.5 and 3.0. The pipe's mass ratio was not altered by changing the geometric or structural properties of the pipe, but by changing the density of the pipe's internal fluid. The model was constructed so that when the pipe was empty $m^* = 1.0$ and when $m^* = 3.0$ the axial tension at the pipe's bottom end was zero. Changing the pipe's mass ratio has the effect of changing its natural frequencies and mode shapes. As m^* is increased the natural frequency, f_n^k where k is the mode number, of a specific mode is reduced. Furthermore as m^* is increased the natural frequencies become more closely spaced.

The axial variation of the pipe's root mean square vibration amplitude, y_{rms}, is presented in Fig. 3 for the $m^* = 1.5$ and 2.5 cases. The axial coordinate, z, measures the distance along the pipe from its bottom end. The pipe's top and bottom ends are located at $z/L = 1$ and $z/L = 0$ respectively. The free surface is coincident with the pipe's top end, i.e., $z/L = 1$.

Clearly the responses of the $m^* = 1.5$ and $m^* = 2.5$ pipes are multi-modal (as are the responses of the remaining cases that are not shown). Note that if a pipe responds in a single mode of vibration then the root mean square displacement at the nodes of that mode would be zero. The response of the $m^* = 1.5$ pipe is dominated by a response in the 5th mode but there is evidently response in other modes. The $m^* = 2.5$ pipe exhibits a similar multi-modal response with a predominant response in the 10th mode. As noted above increasing m^* reduces the pipe's natural frequencies such that given a specific excitation frequency one would expect the mode number of the predominantly excited mode to rise with increasing m^*.

It can be instructive to decompose each pipe's total displacement into its modal contributions. The vector of modal amplitudes, $\mathbf{q}(t)$, is related to the vector of nodal displacements and rotations, $\mathbf{r}(z,t)$, through:

$$\mathbf{q}(t) = \boldsymbol{\Phi}^{-1}(z)\mathbf{r}(z,t), \tag{1}$$

where $\boldsymbol{\Phi} = (\phi^1, \phi^2, \ldots, \phi^M)$ is the mass normalised matrix of eigenvectors and M is the number of unconstrained structural degrees of freedom and hence eigenvectors.

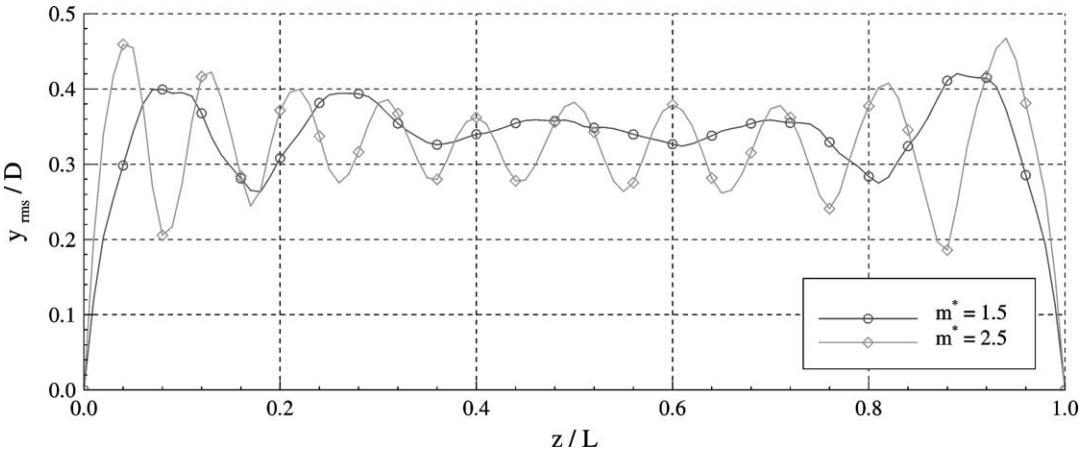

Fig. 3. Root mean square vibration amplitudes, y_{rms}/D, as a function of the pipe's axial coordinate normalised by its length, z/L, for $m^* = 1.5$ and 2.5.

Time histories of the modal displacements for each mass ratio have been determined by solving Eq. (1) at every time step. The root mean squares of the modal displacement histories, y^k_{rms}, are shown in Fig. 4 as a function of each mode's natural frequency normalised upon the vortex shedding (Strouhal) frequency of the stationary cylinder at the same Reynolds number, f_s (as determined by the current numerical method). For example, for $m^* = 1.0$, there is a mode (the 3rd), for which $f^k_n/f_s \approx 0.5$, that vibrates with an rms amplitude of approximately $0.24D$. As noted earlier changing m^* changes the pipe's natural frequencies and mode shapes. Consequently, making comparisons of the responses of different mass ratio pipes in terms of the vibration of specific mode numbers is of limited value. Alternatively, as is done in this paper, the modal vibrations of the different mass ratio pipes can be compared in terms of modal natural frequencies.

It was found that instantaneously loading the pipe had the effect of exciting numerical transients in its response. These manifested themselves as responses in the lowest modes of vibration and could not be damped out within acceptable computation times. The transiently responding (unconverged) modes are plotted in Fig. 4 using open symbols, whilst closed symbols are used to identify converged modes. The numerical transients are most prolific for the higher mass ratio cases but are still not believed to be of serious consequence as they occurred at frequencies far below the response frequencies of the vortex excited modes. For clarity the unconverged modes are omitted from all of the subsequent figures of this paper.

Fig. 4 shows that all of the test cases responded multi-modally. Each simulated response is characterised by a response envelope that extends over several modes and is centred on a single predominant mode. As the mass ratio is reduced the predominantly excited mode occurs at a lower natural frequency, i.e., the peak modal response occurs at a lower f^k_n/f_s as m^* is reduced. Furthermore the amplitude of the predominant mode decreases as m^* is reduced. The width of the excitation envelope increases as the mass ratio is decreased, i.e., as m^* is reduced the fluid is able to excite modes covering a wider natural frequency range. The response is mainly confined to modes whose natural frequencies are below the fluid's natural shedding (Strouhal) frequency, i.e., $f^k_n/f_s < 1$.

For each mass ratio simulated, the oscillatory (response) frequency of each mode, f^k_o, was determined by taking a Fast Fourier Transform of its displacement history. The kth mode's oscillatory frequency was identified as the most energetic frequency in the kth mode's displacement spectrum. The modal oscillatory frequencies are shown in Fig. 5 as a function of the modal natural frequencies. Both sets of frequencies are normalised upon the Strouhal frequency, f_s. Modes that vibrate at their natural frequencies occupy the line $f_o = f_n$. In each case simulated the vortex shedding frequency, $f_v(z)$ (determined as the most energetic frequency in the spectrum of the sectional lift coefficient), was found to be relatively constant with respect to the axial coordinate and occur at or just below the Strouhal frequency, i.e., $f_v(z) \approx f_s$.

As can be seen from the figure, the excited modes, whose natural frequencies are below the excitation frequency ($f^k_n/f_s < 1$) respond above their natural frequencies at a frequency approximately equal to the excitation frequency, i.e., $f^k_o \approx f_s$. These modes are described as locked-in as their oscillatory frequencies are synchronised with the excitation frequency. Modes whose natural frequencies are above the excitation frequency ($f^k_n/f_s > 1$) respond, if they are at all excited, at or just above their natural frequencies, i.e., $f^k_o \approx f^k_n$. Note that there are two misleading data points in Fig. 5: at $f^k_n/f_s \approx 1.47$ for $m^* = 2.0$ and at $f^k_n/f_s \approx 1.93$ for $m^* = 1.0$. The responses of these two modes are insignificant and are comprised of many low amplitude oscillatory frequencies including the excitation frequency.

For $m^* \leqslant 2.0$ Fig. 5 shows that all modes whose natural frequencies are below the excitation frequency are locked-in to the latter frequency. For $m^* > 2.0$, the response envelope does not extend to low enough frequencies to lock-in the lowest modes of

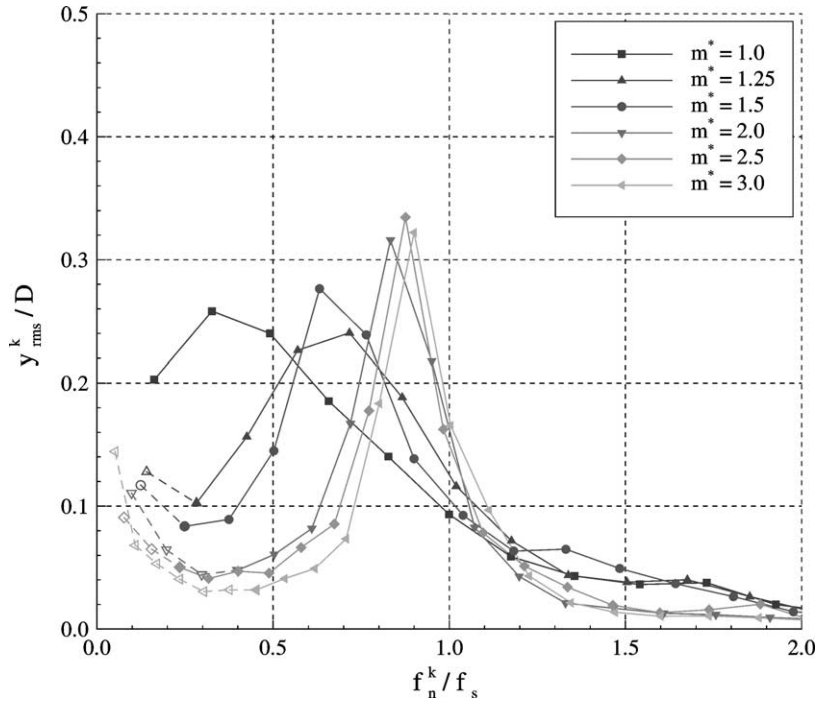

Fig. 4. Modal root mean square vibration amplitudes, y^k_{rms}/D, as a function of modal natural frequencies normalised by the Strouhal frequency, f^k_n/f_s, for $m^* = 1.0$, 1.25, 1.5, 2.0, 2.5 and 3.0. Closed and open symbols signify converged and unconverged modes respectively.

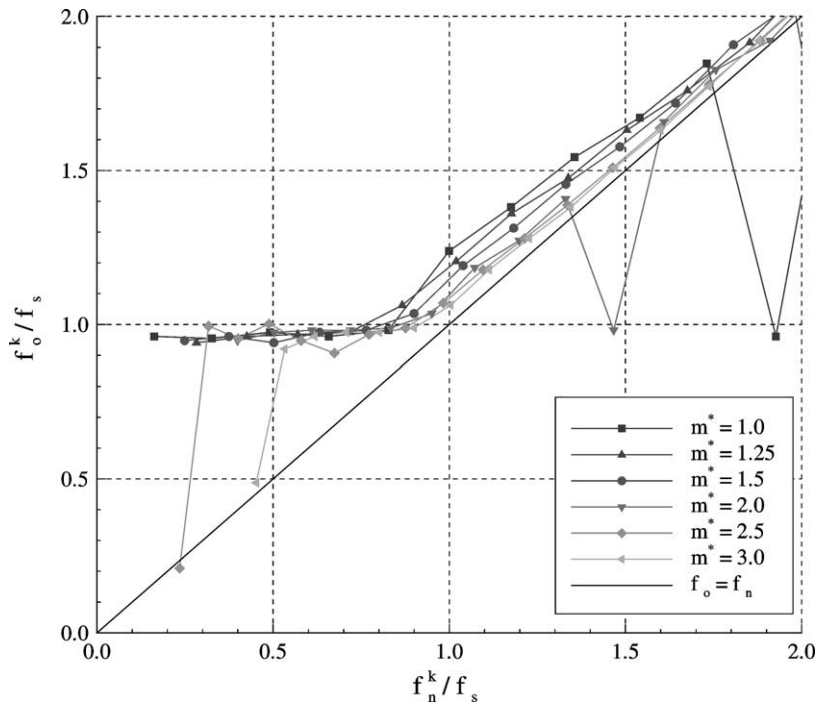

Fig. 5. Modal oscillatory frequencies, f^k_o/f_s, as a function of modal natural frequencies, f^k_n/f_s, for $m^* = 1.0$, 1.25, 1.5, 2.0, 2.5 and 3.0. Both oscillatory and natural frequencies are presented as a fraction of the Strouhal frequency, f_s.

vibration. These modes respond at their natural frequencies, i.e., $f_o^k \approx f_n^k$: see the data points at $f_n^k/f_s \approx 0.24$ for $m^* = 2.5$ and at $f_n^k/f_s \approx 0.45$ for $m^* = 3.0$. The width of the lock-in step, or equivalently the response envelope, decreases with increasing mass ratio. One might expect that at higher mass ratios, where the structure is dominant over the fluid in controlling the response frequency, no such lock-in step would exist and the response would be confined to a single mode of vibration.

The ability of a single degree of freedom low mass ratio cylinder to oscillate away from its natural frequency has been previously observed and explained through changes to the added mass, see, for example, Willden and Graham [16]. The departure of the modal oscillatory frequencies from their natural frequencies can be explained in an analogous manner. The modal equation of motion can be written as:

$$\mathbf{I}\ddot{\mathbf{q}} + \mathbf{C}\dot{\mathbf{q}} + \boldsymbol{\Lambda}\mathbf{q} = \boldsymbol{\Phi}^t\mathbf{R}, \tag{2}$$

where $\dot{\mathbf{q}}$ and $\ddot{\mathbf{q}}$ are the vectors of modal velocities and accelerations. $\mathbf{I}$ is the identity matrix, $\boldsymbol{\Lambda}$ is the diagonal matrix of eigenvalues, $\mathbf{C}$ is the modal damping matrix and $\mathbf{R}$ is the nodal fluid loading vector. $\boldsymbol{\Phi}^t\mathbf{R}$ is referred to as the generalised load vector. The generalised loading of the kth mode can be approximated by:

$$\phi^k \cdot \mathbf{R} \approx -C_a^k\ddot{q}^k - C_v^k\dot{q}^k, \tag{3}$$

where $C_a^k\ddot{q}^k$ and $C_v^k\dot{q}^k$ are the components of the kth mode's generalised fluid loading that are in phase with the kth mode's acceleration and velocity respectively. C_a^k and C_v^k are time independent constants. If the system has reached a steady oscillatory state then the structural damping of the kth mode must be balanced by the $C_v^k\dot{q}^k$ term. C_a^k is defined as the kth mode's added mass coefficient.

The significance of the modal added mass coefficient is that when C_a^k is positive the kth mode must vibrate below its natural frequency, i.e., $C_a^k > 0 \Rightarrow f_o^k < f_n^k$, and when C_a^k is negative the kth mode must vibrate above its natural frequency, i.e., $C_a^k < 0 \Rightarrow f_o^k > f_n^k$. Note that $C_a^k = 1.0$ implies that the added mass associated with the kth mode is equal to the generalised mass of the kth mode. In order that the effective mass of each mode of the combined fluid and structure system remains positive $C_a^k > -1.0$.

C_a^k and C_v^k must be determined such that the right-hand side of Eq. (3) approximates $\phi^k \cdot \mathbf{R}$ as well as possible over some predefined analysis time interval. A residual, ε^k, can be defined to quantify the departure of the kth mode's fluid loading from its approximate representation.

$$\varepsilon^k = \phi^k \cdot \mathbf{R} + C_a^k\ddot{q}^k + C_v^k\dot{q}^k. \tag{4}$$

The integral over the analysis interval of the residual squared measures the approximation's total deviation over the time window of interest. This quantity can be minimised with respect to changes in C_a^k and C_v^k by satisfying:

$$\frac{\partial}{\partial C_a^k}\int_{t_1}^{t_2}\left(\varepsilon^k\right)^2 \mathrm{d}t = 0, \frac{\partial}{\partial C_v^k}\int_{t_1}^{t_2}\left(\varepsilon^k\right)^2 \mathrm{d}t = 0, \tag{5}$$

where t_1 and t_2 are the limits of the analysis interval. Substituting the definition of the residual into these minimisation statements and differentiating yields a set of simultaneous equations that, given records of the modal velocities and accelerations and of the fluid loading, can be solved for C_a^k and C_v^k.

The above procedure has been used to determine a modal added mass coefficient for each mode of vibration. These are plotted against f_n^k/f_s in Fig. 6. In this figure the curve $f_o = f_s$ shows the added mass coefficient, C_a^s, that would be required to force a mode, of natural frequency f_n, to oscillate at the Strouhal frequency. It can be shown that the added mass coefficient required to produce such a behaviour is given by:

$$C_a^s = \left(\frac{f_n}{f_s}\right)^2 - 1. \tag{6}$$

Fig. 6 shows that the excited modes that occupy the lock-in step ($f_n^k/f_s < 1$) have negative added mass coefficients. This enables them to respond above their natural frequencies, i.e., $f_o^k > f_n^k$. Furthermore, each excited mode has an added mass coefficient approximately equal to that required to force oscillation at the Strouhal frequency and hence $f_o^k \approx f_s$ for all modes exhibiting a significant response. The behaviour of the added mass coefficient across the lock-in step is similar for all mass ratios. For $f_n^k/f_s > 1$ the added mass coefficient rarely becomes positive and where it does the associated mode has an insignificant amplitude of vibration.

Another useful way to examine the ability of the fluid to excite mode's whose natural frequencies are not equal to the excitation frequency, and to examine the variation of this ability with mass ratio, is to plot the modal response amplitudes as a function of the reduced velocity, V_r, as in Fig. 7. Each mode's reduced velocity is based on that mode's in vacuo

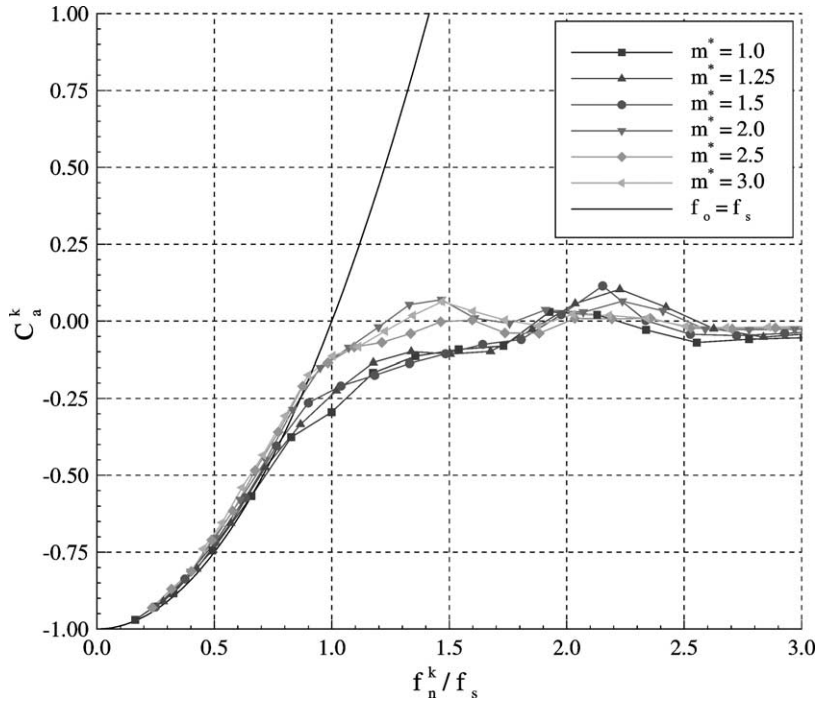

Fig. 6. Modal added mass coefficients, C_a^k, as a function of modal natural frequencies normalised by the Strouhal frequency, f_n^k/f_s, for $m^* = 1.0$, 1.25, 1.5, 2.0, 2.5 and 3.0.

natural frequency, $V_r^k = U/f_n^k D$. Hence, low reduced velocities correspond to high mode numbers and high reduced velocities correspond to low mode numbers. Note that the excitation frequency occurs at $V_r \approx 1/St \approx 5.0$.

Fig. 7 shows that for the highest mass ratio case, $m^* = 3.0$, the response is centred on $V_r \approx 5.6$ and is confined to a relatively narrow reduced velocity range: $4.0 < V_r < 9.0$. As the mass ratio is reduced the response envelope widens and the maximum rms response amplitude decreases. For $m^* < 2.0$ the reduced velocity at which the peak response occurs is significantly greater than $V_r \approx 1/St$, i.e., the predominantly excited mode has a natural frequency that is significantly less than the excitation frequency. At the lowest mass ratio simulated, $m^* = 1.0$, the response envelope extends past $V_r = 30.0$ and encompasses all modes whose natural frequencies are below the excitation frequency. Note that all mass ratios show low amplitude responses for $1.0 < V_r < 2.0$. These high mode responses occur at frequencies between three and four times the excitation frequency and are believed to be excited by components of the fluid force that are observed in the lift coefficient spectra at approximately three to four times the frequency of the vortex shedding.

From Fig. 7 it can be observed that the vibrational behaviour of flexible pipes has much in common with the vibrational behaviour of elastically mounted circular cylinders. For comparative purposes numerically simulated (at lower Reynolds numbers) transverse rms response amplitudes, y_{rms}, of elastically supported circular cylinders of $m^* = 1.0$, 2.0, 5.0 and 10.0 are plotted in Fig. 8 against reduced velocity, $V_r = U/f_n D$ (where f_n is the in vacuo natural frequency of vibration of the cylinders). For these computations the two-dimensional CFD model described earlier (without the LES model) was used to simulate the fluid dynamics whilst a mass, spring and damper model was used to represent the structural dynamics. In all of the cases simulated the structural damping was set to zero. The reduced velocity was varied by changing the flow speed such that the Reynolds number varied linearly with V_r from $Re = 50$ at $V_r = 2.5$ to $Re = 400$ at $V_r = 20.0$.

Similarities in the vibrational behaviours of the elastically supported and flexible cylinders can be deduced by comparing Figs. 7 and 8. In both cases the response envelopes are quite narrow at the highest mass ratios simulated. As m^* is reduced the response envelopes widen and occupy a greater reduced velocity range. For $m^* = 1.0$ both the elastically supported cylinder and flexible pipe exhibit responses at very high reduced velocities. In both cases these high V_r responses occur at frequencies far in excess of the relevant structural in vacuo natural frequency. Note that in Fig. 8 the secondary responses that occur for the $m^* = 5.0$ and 10.0 elastically supported cylinders between $V_r \approx 7.0$ and $V_r \approx 14.0$ are modulated responses. These responses occur at or near to the structure's in vacuo natural frequency but are excited by vortex shedding at or close to the shedding frequency of the stationary cylinder.

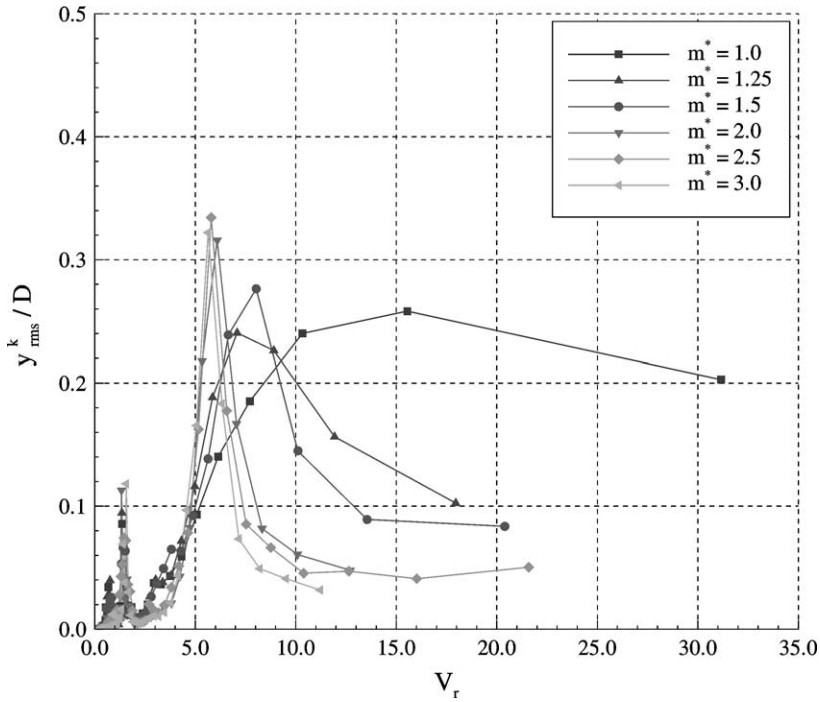

Fig. 7. Modal root mean square vibration amplitudes, y^k_{rms}/D, as a function of modal reduced velocity, $V^k_r = U/f^k_n D$, for $m^* = 1.0$, 1.25, 1.5, 2.0, 2.5 and 3.0.

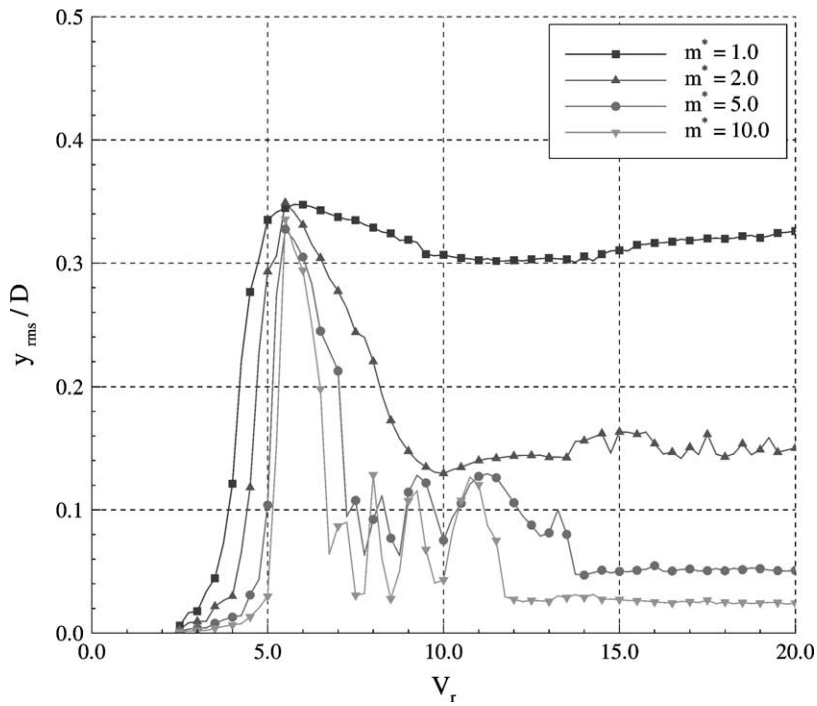

Fig. 8. Root mean square vibration amplitudes, y_{rms}/D, as a function of reduced velocity, $V_r = U/f_n D$, for elastically supported circular cylinders free to vibrate in the transverse direction; $m^* = 1.0$, 2.0, 5.0 and 10.0.

4. Conclusions

It has been shown for mass ratios less than 3.0, that a long flexible pipe, which is subject to a uniform current profile, vibrates multi-modally. Furthermore, the excited modes all respond at the same frequency, being the excitation (Strouhal) frequency. The fluid, via its added mass, is able to force each structural mode to respond at a frequency far from its natural frequency. At these low mass ratios the fluid is dominant over the structure in controlling the response frequency.

The fluid is more able to excite modes that have natural frequencies less than the excitation frequency than those that have natural frequencies exceeding the excitation frequency. The response envelope over which the fluid is able to excite modes whose natural frequencies differ from the excitation frequency decreases with increasing mass ratio. The dependency of the width of the response envelope on the mass ratio is similar to the dependency observed for the transverse vibrations of elastically supported circular cylinders.

Acknowledgements

The authors wish to acknowledge the support of the Engineering and Physical Sciences Research Council (UK), BP Exploration Ltd., Orcina Ltd., BMT Fluid Mechanics Limited and the Department of Trade and Industry (UK).

References

[1] T. Sarpkaya, Vortex-induced oscillations: a selective review, J. Appl. Mech. 46 (2) (1979) 241–258.
[2] P.W. Bearman, Vortex shedding from oscillating bluff bodies, Annu. Rev. Fluid Mech. 16 (1984) 195–222.
[3] G. Parkinson, Phenomena and modelling of flow-induced vibrations of bluff bodies, Prog. Aerosp. Sci. 26 (1989) 169–224.
[4] A. Khalak, C.H.K. Williamson, Motions, forces and mode transitions in vortex-induced vibrations at low mass-damping, J. Fluids Structures 13 (1999) 813–851.
[5] R. Govardhan, C.H.K. Williamson, Modes of vortex formation and frequency response of a freely vibrating cylinder, J. Fluid Mech. 420 (2000) 85–130.
[6] R.H.J. Willden, J.M.R. Graham, Numerical simulation of the flow about deep water riser pipes, in: T. Kvamsdal, I. Enevoldsen, K. Herfjord, C. Jenssen, K. Mehr, S. Nørsett (Eds.), Computational Methods for Fluid–Structure Interaction, Tapir, Trondheim, 1999, pp. 315–324.
[7] R.H.J. Willden, Numerical prediction of the vortex-induced vibrations of marine riser pipes, Ph.D. thesis, University of London, UK, 2003.
[8] D.J. Newman, G.E. Karniadakis, A direct numerical simulation study of flow past a freely vibrating cable, J. Fluid Mech. 344 (1997) 95–136.
[9] C.H.K. Williamson, Vortex dynamics in the cylinder wake, Annu. Rev. Fluid Mech. 28 (1996) 477–539.
[10] G.H. Toebes, The unsteady flow and wake near an oscillating cylinder, ASME J. Basic Engrg. 91 (1969) 493–502.
[11] J.M.R. Graham, Computation of viscous separated flow using a particle method, in: K.W. Morton, M.J. Baines (Eds.), Numerical Methods for Fluid Dynamics III, in: Inst. Math. Appl. Conf. Ser., vol. 17, Oxford University Press, 1988, pp. 310–317.
[12] J. Smagorinsky, General circulation experiments with the primitive equations, part 1: the basic experiment, Monthly Weather Rev. 91 (1963) 99–164.
[13] C. Norberg, Flow around a circular cylinder: Aspects of fluctuating lift, J. Fluids Structures 15 (2001) 459–469.
[14] R.H.J. Willden, J.M.R. Graham, CFD simulations of a model steel catenary riser undergoing simultaneous in-plane and out-of-plane vortex-induced vibrations, Tech. rep., STRIDE JIP Ph. IV, 2002.
[15] MARINTEK, VIV model test of a catenary riser, Tech. Rep. 512345.00.01 rev.01, STRIDE JIP Ph. IV, 2002.
[16] R.H.J. Willden, J.M.R. Graham, Numerical prediction of VIV on long flexible circular cylinders, J. Fluids Structures 15 (2001) 659–669.